JACS
JOURNAL OF THE AMERICAN CHEMICAL SOCIETY
Article
pubs.acs.org/JACS

An Exceptionally Stable Metal–Organic Framework Supported Molybdenum(VI) Oxide Catalyst for Cyclohexene Epoxidation

Hyunho Noh,[†] Yuexing Cui,[†] Aaron W. Peters,[†] Dale R. Pahls,[‡] Manuel A. Ortuño,[‡] Nicolaas A. Vermeulen,[†] Christopher J. Cramer,*[,‡] Laura Gagliardi,*[,‡] Joseph T. Hupp,*[,†] and Omar K. Farha*[,†,§]

[†]Department of Chemistry and Chemical and Biological Engineering, Northwestern University, 2145 Sheridan Road, Evanston, Illinois 60208, United States

[‡]Department of Chemistry, Supercomputing Institute, and Chemical Theory Center, University of Minnesota, Minneapolis, Minnesota 55455, United States

[§]Department of Chemistry, Faculty of Science, King Abdulaziz University, Jeddah 21589, Saudi Arabia

Supporting Information

ABSTRACT: Molybdenum(VI) oxide was deposited on the Zr_6 node of the mesoporous metal–organic framework NU-1000 via condensed-phase deposition where the MOF is simply submerged in the precursor solution, a process named solvothermal deposition in MOFs (SIM). Exposure to oxygen leads to a monodisperse, porous heterogeneous catalyst, named **Mo-SIM**, and its structure on the node was elucidated both computationally and spectroscopically. The catalytic activity of **Mo-SIM** was tested for the epoxidation of cyclohexene. Near-quantitative yields of cyclohexene oxide and the ring-opened 1,2-cyclohexanediol were observed, indicating activity significantly higher than that of molybdenum(VI) oxide powder and comparable to that of a zirconia-supported analogue (Mo-ZrO_2) prepared in a similar fashion. Despite the well-known leaching problem of supported molybdenum catalysts (i.e., loss of Mo species thus causes deactivation), **Mo-SIM** demonstrated no loss in the metal loading before and after catalysis, and no molybdenum was detected in the reaction mixture. In contrast, Mo-ZrO_2 led to significant leaching and close to 80 wt % loss of the active species. The stability of **Mo-SIM** was further confirmed computationally, with density functional theory calculations indicating that the dissociation of the molybdenum(VI) species from the node of NU-1000 is endergonic, corroborating the experimental data for the **Mo-SIM** material.

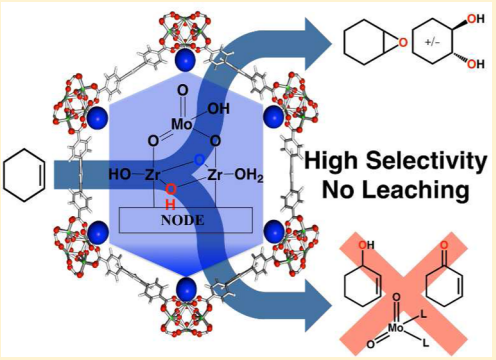

INTRODUCTION

Metal–organic frameworks (MOFs), simultaneously possessing porosity and crystallinity,[1−6] have attracted significant attention as heterogeneous catalysts[6−10] and scaffolds on which to deposit externally introduced catalytic species.[11−23] Rational designs of both the inorganic node and the organic linker allow substantial structural freedom within a confined chemical environment.[4−6] In particular, MOFs with free hydroxyl groups have attracted much attention due to their potential to anchor catalysts in an analogous manner to traditional metal-oxo supports (e.g., alumina, zirconia, or silica).[11−15,24] These catalysts have long played a central role as heterogeneous catalysts applicable to industrial-scale syntheses.[25−27] Yet, the exact structure and location of the metal catalysts, and the involved catalytic mechanisms, are difficult to probe due to the phenomenon known as the "support effect".[11,28,29] In traditional amorphous material, the hydroxyl groups exploited for anchoring active species possess various Lewis and/or Brønsted acidities, local densities, and binding motifs. Consequently, the structure and the surrounding chemical environment of the catalyst are often challenging to predict or manipulate.[11] In contrast, the discrete grafting sites provided by the isolated metal oxide/hydroxide nodes of MOFs offer the potential to produce structurally characterizable heterogeneous catalysts.[1−6] We[11−15,19,24] and others[21−23,30,31] have exploited impregnation of metal-containing species in MOFs and have successfully prepared transition metal-based heterogeneous catalysts, both in the vapor phase via atomic layer deposition (ALD) in MOFs (AIM)[11−13,24] and in condensed phase via solvothermal deposition in MOFs (SIM).[14,15,19,31]

Here we explore the deposition of a catalytically active molybdenum(VI) oxide on the node of a MOF by SIM.[32,33] Homogeneous oxomolybdenum species have demonstrated high conversion and selectivity for the synthesis of epoxides.[34−37] Traditionally, these catalysts suffer from deactivation by μ-oxo oligomerization.[36,37] Deposition of the Mo catalyst on a silica[38−41] or alumina[42,43] support suppresses

Received: August 24, 2016
Published: October 25, 2016

DOI: 10.1021/jacs.6b08898
J. Am. Chem. Soc. 2016, 138, 14720−14726

such deactivation on the surface; however, the active species commonly leaches out of the support, and hence the stability is a challenging problem yet to be fully resolved.[34,35,37] To our understanding, the exact mechanism behind the leaching process (i.e., loss of Mo species via cleavage from the support) remains to be deconvoluted due to the structural ambiguity of the active species. Motivated by this problem, we decided to deposit molybdenum(VI) oxide in a MOF, specifically NU-1000.

NU-1000, which consists of eight-connected $Zr_6(\mu_3\text{-}O)_4(\mu_3\text{-}OH)_4(H_2O)_4(OH)_4$ nodes[44] connected by 1,3,5,8-(*p*-benzoate)pyrene linkers ($TBAPy^{4-}$)[45] was specifically chosen as the platform for the molybdenum(VI) oxide deposition. It has a well-defined crystal structure[44] and the proton topology of the nodes is well understood.[46] In addition, NU-1000 is thermally and chemically stable.[47] The hierarchical structure of NU-1000, with micro- and mesoporosity and pore sizes of 10 and 31 Å, allows efficient diffusion of substrates and ready access to designed active sites (Figure 1).[48,49]

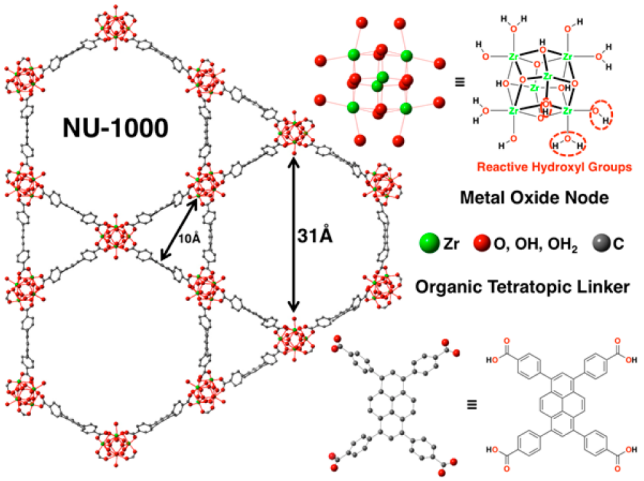

Figure 1. Nonmetalated NU-1000 with pore sizes and structures of metal oxide node and organic linker. Three of the 12 anchoring sites upon metalation are shown on the node.

RESULTS AND DISCUSSION

Mo-SIM Synthesis. The detailed synthesis of **Mo-SIM** is outlined in the Methods section. SIM was implemented due to its facile three-step preparation: (1) metalation, (2) exposure to oxygen, and (3) activation. Commercially available bis(*tert*-butylimido)bis(dimethylamino)molybdenum(VI) ($Mo(am)_2(im)_2$) was chosen as the molybdenum precursor as the compound is stable under air- and water-free environments, but readily reacts upon exposure to hydroxyl groups to form the metal oxide and benign byproduct (*tert*-butyl amine and dimethyl amine). Subsequent exposure to oxygen leads to a site-isolated heterogeneous molybdenum(VI) oxide catalyst.

Characterization of Mo-SIM. Small decreases in Brunauer–Emmett–Teller (BET) surface area from 2100 to 1800 m^2/g and pore volume from 1.4 to 1.2 cm^3/g were observed for **Mo-SIM** relative to bare NU-1000. The isotherm clearly shows the type IVc feature, associated with the mesoporosity of NU-1000,[24,49] suggesting that the framework remained intact (Figure 2). The decrease in density function theory (DFT)-calculated average pore width of **Mo-SIM** (Figure S1) was observed for the hexagonal pores (i.e., from 29 to 27 Å). From

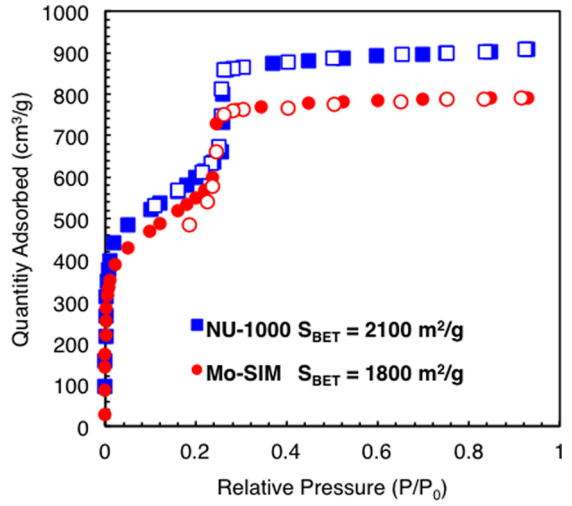

Figure 2. N_2 isotherm of NU-1000 and **Mo-SIM** with every other data point plotted. Adsorption and desorption are represented by filled and unfilled points, respectively.

the thermogravimetric analysis (TGA) graph, 24% weight loss difference at 700 °C between **Mo-SIM** and NU-1000 was observed. We attribute this difference in weight loss to molybdenum oxide, which remained with the decomposed framework, thus leading to smaller decrease in mass with respect to its initial mass (Figure S2). Scanning electron microscopy (SEM) images exhibited no morphological change of the parent framework upon metal deposition, and the energy-dispersive spectroscopy (EDS) line scan was used to confirm uniform dispersion of the molybdenum species throughout the crystal (Figure S3). Inductively coupled plasma optical emission spectroscopy (ICP-OES) measurements showed the metal loading of 2.8 ± 0.3 Mo/Zr_6 node.

In the diffuse reflectance infrared Fourier transform (DRIFT) spectrum of **Mo-SIM** (Figure S4), a decrease in intensity of the peak associated with terminal and bridging −OH stretches on the node at 3674 cm^{-1} relative to NU-1000 was confirmed, suggesting a chemisorption of Mo species on the node, as shown previously.[24] The new emerging peak at 3660 cm^{-1} was attributed to −OH stretch attached to Mo. In the Raman spectrum of **Mo-SIM** (Figure S5), a small broad peak at 922 cm^{-1} attributed to the terminal Mo═O stretch[50−52] was confirmed. The Raman spectra of MoO_3 and Na_2MoO_4 show peaks at 820 and 840 cm^{-1}, attributed to the stretch by Mo−O−Mo moieties, and thus suggest oligomerization.[50−52] Though this stretch is not apparent in the **Mo-SIM** spectrum, potential overlap with peaks associated with NU-1000 cannot be ruled out.

X-ray absorption spectroscopy (XAS) was employed to further elucidate the structure of the Mo species in NU-1000. In the X-ray absorption near edge structure (XANES) region (Figure 3a), the edge energy (corresponding to a 1s-to-5p transition) of both **Mo-SIM** and MoO_3 was measured to be 20 006 eV, while that of MoO_2 was 20 005 eV. The pre-edge energy, associated with the 1s-to-4d transition, was measured to be 1 eV lower for **Mo-SIM** than MoO_3 (19 996 and 19 997 eV, respectively), typically associated with the distortion of the preferred octahedral geometry to a more tetrahedral symmetry.[53,54] Thus, we conclude that the Mo species deposited are fully oxidized to a Mo(VI) with a tetrahedral local symmetry. The oxidation state of the species was further

DOI: 10.1021/jacs.6b08898
J. Am. Chem. Soc. 2016, 138, 14720−14726

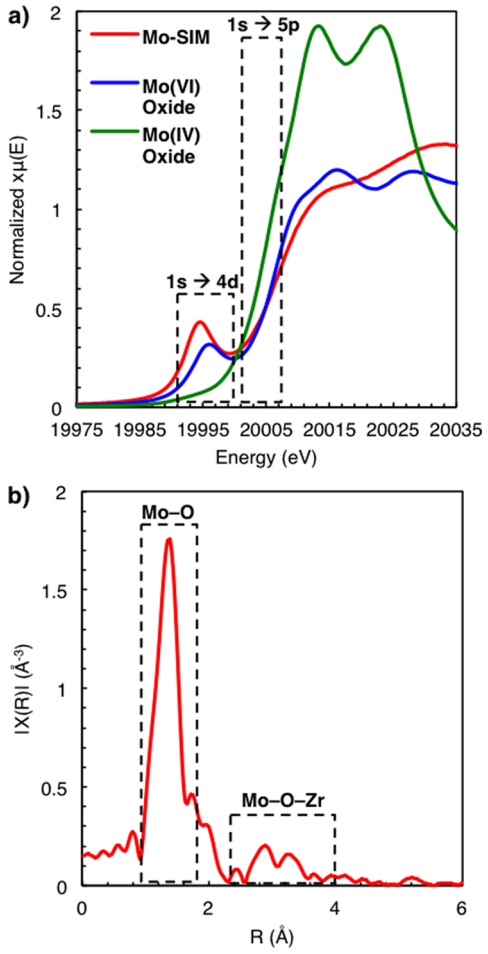

Figure 3. (a) XANES of **Mo-SIM**, MoO_3, and MoO_2 and (b) EXAFS of **Mo-SIM** that justify the presence of monomeric nature of Mo species with tetrahedral symmetry. Note that Mo−O−Mo scattering signal overlaps with that of Mo−O−Zr, so small amounts of oligomeric Mo species may not be detected. For details, see Figure S8.

confirmed by X-ray photoelectron spectroscopy (XPS) (Figure S6). In the extended X-ray absorption fine structure (EXAFS) region (Figure 3b), Mo−O and Mo−O−Zr scatterings were confirmed, suggesting Mo species to be monomeric, or at most few Mo atom clusters.

Density functional theory (M06-L functional, see Methods section for full details) calculations were performed to characterize the structures and energetics of various Zr_6 nodes modified supporting mono- and binuclear molybdenum complexes. For the node itself, a cluster model comprised of the Zr_6 node itself with eight truncated linkers was adopted, and many different mono- and binuclear Mo complexes were constructed by anchoring Mo(VI) atoms to oxygen functionality of the Zr_6 node, and then adding oxide and/or hydroxide ligands, and/or losing node protons, to achieve charge balance and a coordination number of at least 4 for all Mo atoms. Lowest energy species were identified from this procedure and we now discuss them in more detail.

From a number of possible monometallic structures considered, the three shown in Figure 4a (**Mo-1**−**Mo-3**) had the lowest relative free energies. All possess Mo—OH and/or Mo═O bonds, in agreement with the DRIFT and Raman spectra, respectively, noted above. These most favorable structures all have tetrahedral, rather than octahedral,

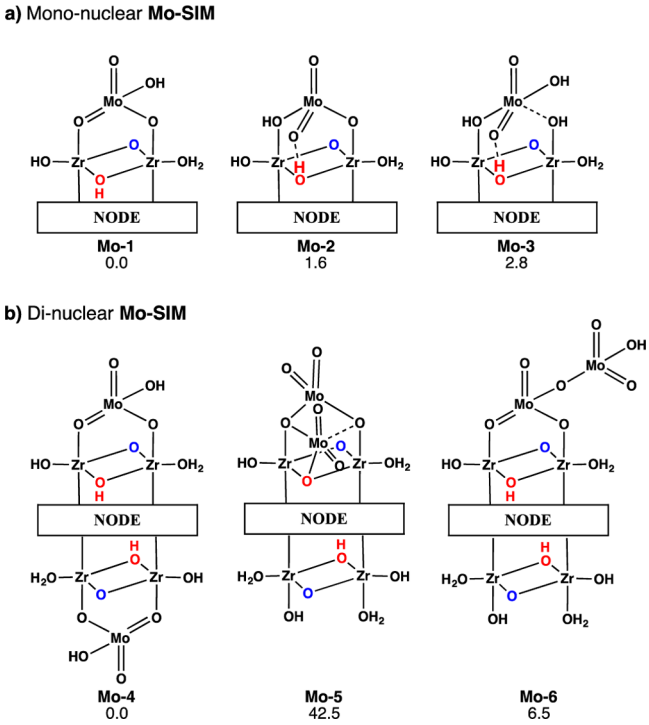

Figure 4. (a) Three energetically accessible monomolybdenum structures **Mo-1**−**Mo-3**, and (b) three dimolybdenum species, **Mo-4**−**Mo-6**, with their associated relative free energies. For other structures, see SI. ΔG_{tol} in kcal/mol.

coordination environments, which is consistent with the XANES measurements. Systems containing two molybdenum centers with Mo−O−Mo bonding motifs bound to one face of the node were compared to a system where the two molybdenum atoms bind to two different faces of the Zr_6 node (Figure 4b). **Mo-4** is the most stable structure of the three and would not show Mo−O−Mo scattering. Deposition of molybdenum onto PCN-700, a related Zr_6 MOF, also showed one molybdenum per face.[32] Therefore, we conclude that the secondary scattering peaks of **Mo-SIM** in the EXAFS region are primarily associated with Mo−O−Zr scattering, further supporting the site-isolated nature of **Mo-SIM**.

Cyclohexene Epoxidation. Since Mo-based catalysts have long been understood to have catalytic activity toward epoxidation,[34−37] **Mo-SIM** is an appropriate candidate catalyst for cyclohexene epoxidation. Details of the reaction conditions can be found in the Methods section and the Supporting Information (SI). The reaction can proceed via two mechanisms: direct and radical pathways. As shown in Scheme 1, possible products are cyclohexene oxide, 2-cyclohexenol, 2-cyclohexenone, and *trans*-1,2-cyclohexanediol (racemic mixture). **Mo-SIM** exhibited a high conversion of 93 ± 2% after 7 h of reaction at 60 °C under N_2 atmosphere upon optimization of the reaction condition with 0.5 mol % catalyst and 2 equiv of the oxidant relative to cyclohexene. A very high selectivity of 99 ± 1% for cyclohexene epoxide and the ring-opened diol (Figure 5, Table 1) was measured. Leus et al.[55] have proposed the generation of water during this catalysis, which then initiates the epoxide ring opening. Since no other mechanisms to generate the diol have been reported, these two products were considered to derive from the same elementary path.[11,26,27,55] The parent MOF framework without chemisorbed Mo species was observed to have a significantly lower yield of 5 ± 3% (and

DOI: 10.1021/jacs.6b08898
J. Am. Chem. Soc. 2016, 138, 14720−14726

Scheme 1. Reaction Scheme of Cyclohexene Epoxidation

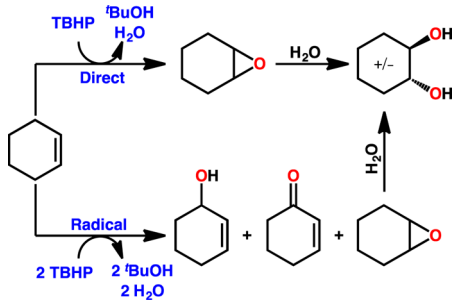

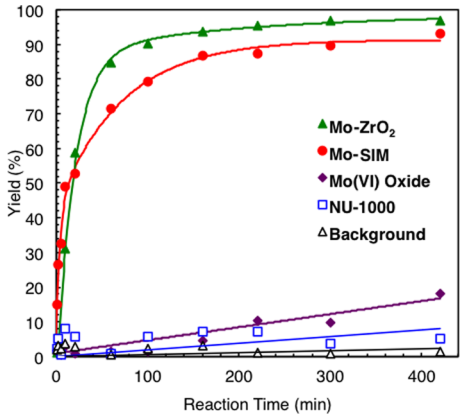

Figure 5. Cyclohexene oxide and 1,2-cyclohexanediol yield vs reaction time of **Mo-SIM**, Mo-ZrO_2, MoO_3, NU-1000, and background (no MOF). For graphs with error bars, see SI.

Table 1. Yield, Selectivity, and Turnover Frequency (TOF) of Mo-SIM, Mo-ZrO_2, MoO_3, NU-1000, and Background for Cyclohexene Epoxidation

conditions	yield (%)[a]	selectivity (%)[a]	TOF (min^{-1})
Mo-SIM	93 ± 2	99 ± 1	7 ± 2[b]
Mo-ZrO_2	97 ± 1	99 ± 1	8 ± 1[b]
MoO_3	22 ± 9	80 ± 9	0.3 ± 0.3[b]
NU-1000	5 ± 3	86 ± 6	–[c]
background	1.5 ± 0.1	36 ± 6	–[c]

[a]Values at 420 min. [b]For TOF, assumed catalyst was 100% of the Mo species. [c]Background and NU-1000 TOFs were difficult to measure.

never above 8 ± 3%) after 420 min, which is marginally larger compared to that of reaction without any additive at all (1.5 ± 0.1% yield). Thus, the catalytic activity of **Mo-SIM** can be solely attributed to the deposited molybdenum species.

Bulk MoO_3 and Mo supported on zirconia (Mo-ZrO_2) were subjected to the same reaction conditions. For details of the synthesis of Mo-ZrO_2, refer to the Methods section. Equimolar amounts of MoO_3 powder showed a lower yield of 18 ± 9% with a selectivity of 80 ± 10%. Oligomerization, confirmed by the aforementioned Raman spectrum, lowers the concentration of the active species and may have led to such low yield relative to **Mo-SIM**. Mo-ZrO_2 exhibited a yield of 97 ± 1% with a selectivity of 99 ± 1%. While this system had marginally higher yield, significant leaching of the catalytic species was confirmed via ICP-OES measurements and a leaching test (Figure 6). In particular, wt % loss of 79 ± 1% was observed after the initial reaction. When the catalyst was filtered after 60 min (corresponding to a yield of 75%), the reaction continued in the filtrate solution albeit more slowly than reaction in the

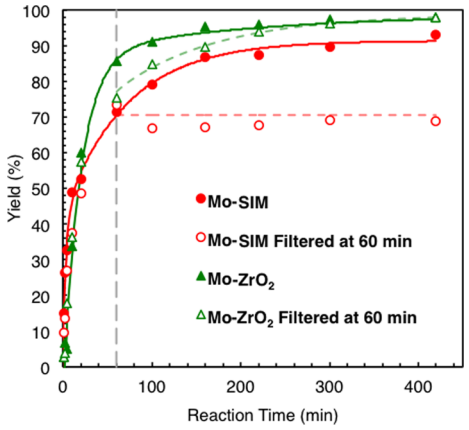

Figure 6. Leaching test of **Mo-SIM** and Mo-ZrO_2. No catalytic species in the filtrate of **Mo-SIM** was observed while the filtrate of Mo-ZrO_2 continued to catalyze cyclohexene epoxidation up to 97% yield. Error bars are omitted for clarity (see SI).

original heterogeneous system, with the yield eventually reaching 97% after 420 min. Thus, the catalytic activity of Mo-ZrO_2 derives from a combination of heterogeneous and homogeneous catalysis. When **Mo-SIM** was filtered at 60 min at 60 °C, by contrast, the catalysis was fully arrested; i.e., no active catalyst leaches into solution. The ICP-OES measurements of **Mo-SIM** before and after catalysis remained consistent as 2.8 ± 0.3 Mo per node, demonstrating exceptional stability of molybdenum(VI) oxide following deposition in NU-1000. Further supporting the stability of **Mo-SIM** is its recyclability as no decrease in yield was confirmed within three cycles. Mo-ZrO_2, however, had a significant decrease in its yield to 30 ± 10% at its third cycle (Figure S11). **Mo-SIM** was determined to maintain its morphology and monodispersity as judged by SEM images and EDS line scans, respectively (Figure S3). Powder X-ray diffraction (PXRD) patterns (Figure 7) show the framework remains crystalline; the patterns correspond to the literature,[12−14,16,38] both upon SIM and after catalysis, confirming the robustness of NU-1000.

To test the versatility of **Mo-SIM** as an epoxidation catalyst, two other substrates, 1-hexene and *cis*-cyclooctene, were tested

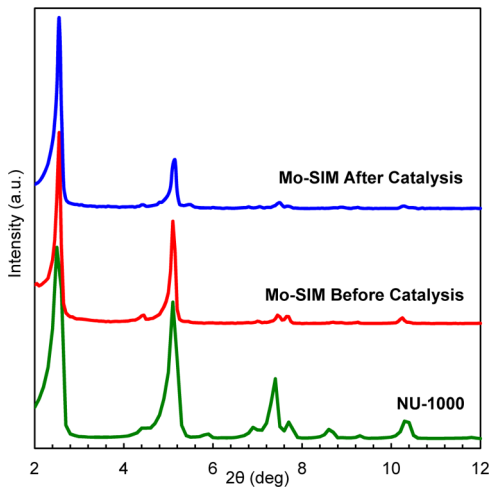

Figure 7. PXRD patterns of NU-1000 and **Mo-SIM** before and after cyclohexene epoxidation. The parent framework stays intact upon metal deposition and during catalysis.

DOI: 10.1021/jacs.6b08898
J. Am. Chem. Soc. 2016, 138, 14720−14726

under the same conditions (for experimental details, see the SI). In both cases, **Mo-SIM** significantly outperformed Mo-ZrO_2, the parent framework, and with no additives with the yield of 55 ± 4% and 99.8 ± 0.2% of 1-hexene oxide and *trans*-1,2-hexanediol, and cyclooctene oxide and *trans*-1,2-cyclooctanediol, respectively (Figures S12−S15, Tables S1 and S2). The selectivity in both reactions were greater than 99%. Mo-ZrO_2 drastically decreased its catalytic activity upon changing the substrate with the yield of 38 ± 4% and 24 ± 5% for 1-hexene and cyclooctene epoxidations, respectively. **Mo-SIM**, again, demonstrated its stability where no leaching was confirmed (Figures S13 and S15). Mo-ZrO_2, on the other hand, lost 55 ± 3 and 50 ± 1 wt % for 1-hexene, and cyclooctene epoxidation, respectively. Furthermore, **Mo-SIM** and Mo-ZrO_2 were both subjugated to cyclohexene epoxidation in acetonitrile, a more polar solvent. Though a decrease in yield was confirmed for both systems, **Mo-SIM** outperforms **Mo-ZrO_2** by close to 20% in yield (Figure S16, Table S3). Despite low performance, Mo-ZrO_2 lost 71 ± 2 wt % after a single run, **Mo-SIM** had minimal leaching of 0.29 ± 0.02 Mo/Zr_6. For all reactions mentioned above, **Mo-SIM** retained its crystallinity (Figure S17), further demonstrating its stability.

To further understand the stability of the chemisorbed Mo species, the thermodynamics of the leaching was calculated at the DFT level. For this calculation, the most stable structure **Mo-1** was considered (Figure 4). As shown in Figure 8,

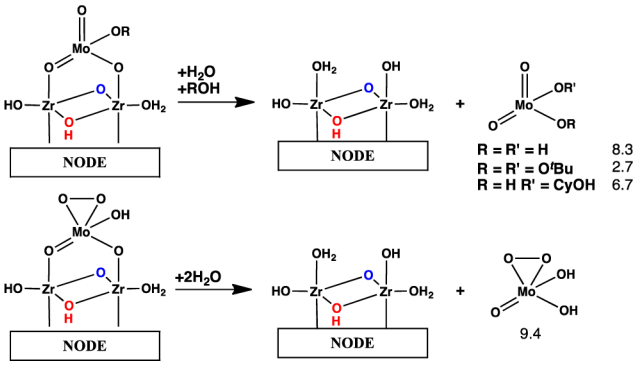

Figure 8. Thermodynamics of the leaching process of **Mo-SIM**. ΔG_{tol} in kcal/mol.

regeneration of the nonmetalated Zr_6 node via reaction with two H_2O molecules under the reaction conditions is predicted to be endergonic by 8.3 kcal/mol. To mimic the catalytic conditions, other complexes were considered that might be formed by ligand exchange that may also promote leeching of molybdenum. The exchange reactions with $M(O)_2(OH)_2$ were explored (see Figure S20) and structures bound to NU-1000 corresponding to the most exoergic exchange reactions were calculated, i.e., peroxo (−OOtBu) and alkoxide (−OCyOH). The leaching of a κ_2-peroxo complex was also calculated as κ_2-peroxo complexes are well-known intermediates for olefin epoxidation.[35] Leaching of all Mo species considered in Figure 8 is still found to be energetically unfavorable by at least 2.7 kcal/mol.[56] Thus, the endergonic nature associated with the leaching of molybdenum, regardless of its ligands, allows **Mo-SIM** to be a stable catalyst for cyclohexene epoxidation.

CONCLUSION

A robust molybdenum(VI) oxide-deposited metal−organic framework, **Mo-SIM** was prepared in a simple three-step synthesis. The extent and potential structure of molybdenum species were elucidated both computationally and experimentally via XAS measurements, DRIFT and Raman spectra, and ICP-OES measurements, supported by DFT calculations. Not only does **Mo-SIM** achieve a high conversion of 93 ± 2%, which is close to that of a bulk zirconia-supported analogue, but it also exhibits exceptional stability where no leaching of the active species and no loss in yield upon recycling were detected, crucial factors for a heterogeneous catalyst that are lacking for Mo-ZrO_2. Furthermore, a precise understanding of the structure of the Zr_6 node permits ready prediction of the active species and rationalization of its/their stability via *in silico* calculations of the thermodynamics of the leaching process, again a factor difficult or even impossible to achieve for the zirconia-supported counterpart, given the ambiguity of its structure. Our calculations show that, in **Mo-SIM**, the Mo leaching is endergonic, regardless of its ligands, allowing **Mo-SIM** to be a stable catalyst for cyclohexene epoxidation. This may, in turn, facilitate further molecular engineering of more stable molybdenum species for deposition, with the goal of preparing structurally uniform, yet highly active, heterogeneous catalysts for alkene epoxidation.

METHODS

NU-1000 Synthesis. NU-1000 was synthesized according to the procedure by Wang et al.[49] N_2 isotherm and PXRD patterns were used for confirming its porosity (i.e., BET surface area and pore size distribution), and crystallinity, respectively.

Mo-SIM Synthesis. SIM was performed by submerging 100 mg (0.05 mmol of Zr_6 node) of NU-1000 into a solution of 120 mg (0.37 mmol) of $Mo(am)_2(im)_2$ (Strem, 98%) in 16 mL of anhydrous heptane (Aldrich, 99%) at room temperature in an argon-filled glovebox and left overnight. The sample was washed with fresh heptane until the supernatant was colorless. The sample was exposed to air, centrifuged to remove excess heptane, and heated under vacuum for 80 °C followed by 120 °C overnight. The molybdenum loading was confirmed by SEM-EDS line scan and ICP-OES measurements. 100 mg of molybdenum-deposited high surface area zirconia (Mo-ZrO_2) was prepared by adding the support to a solution of 13 mg (0.04 mmol) in 16 mL of heptane to achieve close to same wt % as **Mo-SIM** calculated from the ICP-OES measurements. The sample was washed and dried in a similar fashion to **Mo-SIM**. The zirconia support was synthesized according to the procedure reported previously.[57] DRIFTS, TGA, Raman spectroscopy, and XPS were used to further characterize the deposited species. XAS Mo K-edge (20000 eV) scans of **Mo-SIM** and standards were all performed at Argonne National Laboratory. Details of all measurements are given in the SI.

Cyclohexene Epoxidation. This is a modified version of the protocol reported by Leus et al.[55] The radical inhibitor in cyclohexene (Aldrich, ≥99.0%) was removed using activated alumina. Into a 2−5 mL Biotage microwave process vial, 0.3 mL of cyclohexene in 1.75 mL of toluene (Fischer, 99.9%) with 10 mg of **Mo-SIM** was submerged. The mixture was purged under N_2 for 1 min and heated with mechanical stirring at 60 °C for 10 min. Two molar equivalence (relative to cyclohexene) of *tert*-butyl hydroperoxide (TBHP) (Aldrich, 5.5 M in decane) was injected. Reaction kinetics were monitored via analysis of the extracted aliquots at given times and running it through GC-FID (see SI for details). Kinetics of the background reaction, where no MOF is present, reactions solely with 10 mg of NU-1000, MoO_3 powder (Aldrich, ≥99.5%), and Mo-ZrO_2 were monitored in a similar fashion. Leaching tests for **Mo-SIM** and Mo-ZrO_2 were conducted by removing the catalyst after 60 min. The filtrate was placed inside the microwave vial, purged under N_2, and heated at 60 °C to monitor its kinetics. Postsynthetic characterizations (PXRD, SEM-EDS, and ICP-OES) and recyclability tests were

DOI: 10.1021/jacs.6b08898
J. Am. Chem. Soc. 2016, 138, 14720−14726

conducted after the solvent exchange of the catalyst with acetone (see SI).

Computational Modeling. *Model.* A neutral cluster model formed by one node and eight organic linkers was extracted from periodic density functional theory (DFT) calculations.[44] The so-called mixed proton topology was used to describe the node, i.e., $[Zr_6(\mu_3\text{-}O)_4(\mu_3\text{–}OH)_4(OH)_4(OH_2)_4]^{8+}$. The eight $TBAPy_4^-$ (1,3,6,8-tetrakis(*p*-benzoate)pyrene) linkers were truncated so as to retain only coordinating benzoate groups, thereby increasing computational efficiency while maintaining overall charge balance. During the geometry optimization, the organic linkers were kept fixed to account for the rigidity of the solid structure.

Methodology. All calculations were performed at the DFT level using the M06-L functional[58] as implemented in Gaussian 09.[59] The M06-L functional has shown good performance for dispersion interactions, transition metal chemistry,[60,61] and zeolites.[62] Numerical integrations were performed with an ultrafine grid. An automatic density-fitting set generated by the Gaussian program was employed to reduce the computational cost. The 6-31G(d) basis set was used for H, C, and O;[63,64] the SDD pseudopotential and its associated double-ζ basis set was employed for Mo and Zr.[65] All geometry optimizations were performed in the gas phase. The natures of all minima were confirmed by analytic computation of vibrational frequencies at 298.15 K. Final Gibbs energies in solution were computed by adding Gibbs energy contributions in the gas phase to single-point calculations in toluene solvent using the SMD model.[66] Finally, a factor of $RT \times \ln(24.46)$ was added to account for the 1 atm to 1 M standard-state change.

■ ASSOCIATED CONTENT

Supporting Information

The Supporting Information is available free of charge on the ACS Publications website at DOI: 10.1021/jacs.6b08898.

Detailed materials synthesis, characterization data, and computational details; Figures S1–S20 and Tables S1–S3 (PDF)

■ AUTHOR INFORMATION

Corresponding Authors

*cramer@umn.edu
*gagliard@umn.edu
*j-hupp@northwestern.edu
*o-farha@northwestern.edu

Notes

The authors declare no competing financial interest.

■ ACKNOWLEDGMENTS

The authors gratefully acknowledge financial support from the Inorganometallic Catalyst Design Center, an EFRC funded by the U.S. DOE, Office of Basic Energy Sciences (DE-SC0012702). This work made use of the J.B. Cohen X-ray Diffraction Facility, supported by the MRSEC program of the National Science Foundation (DMR-1121262), at the Materials Research Center of Northwestern University. This work also made use of the EPIC and Keck-II facilities (NUANCE Center-Northwestern University), which received support from the MRSEC program (NSF DMR-1121262) at the Materials Research Center; the International Institute for Nanotechnology (IIN); and the State of Illinois, through the IIN. Use of the Advanced Photon Source is supported by the U.S. Department of Energy, Office of Science, and Office of Basic Energy Sciences, under Contract DE-AC02-06CH11357. Materials Research Collaborative Access Team (MRCAT, Sectors 10ID) operations are supported by the Department of Energy and the MRCAT member institutions.

■ REFERENCES

(1) Li, H.; Eddaoudi, M.; O'Keeffe, M.; Yaghi, O. M. *Nature* **1999**, *402*, 276–279.
(2) Rosi, N. L.; Eckert, J.; Eddaoudi, M.; Vodak, D. T.; Kim, J.; O'Keeffe, M.; Yaghi, O. M. *Science* **2003**, *300*, 1127–1129.
(3) Kitagawa, S.; Kitaura, R.; Noro, S. *Angew. Chem., Int. Ed.* **2004**, *43*, 2334–2375.
(4) Li, J.-R.; Kuppler, R. J.; Zhou, H.-C. *Chem. Soc. Rev.* **2009**, *38*, 1477–1504.
(5) Murray, L. J.; Dinca, M.; Long, J. R. *Chem. Soc. Rev.* **2009**, *38*, 1294–1314.
(6) Lee, J.; Farha, O. K.; Roberts, J.; Scheidt, K. A.; Nguyen, S. T.; Hupp, J. T. *Chem. Soc. Rev.* **2009**, *38*, 1450–1459.
(7) Ma, L.; Falkowski, J. M.; Abney, C.; Lin, W. *Nat. Chem.* **2010**, *2*, 838–846.
(8) Ma, L.; Abney, C.; Lin, W. *Chem. Soc. Rev.* **2009**, *38*, 1248–1256.
(9) Liu, Y.; Howarth, A. J.; Hupp, J. T.; Farha, O. K. *Angew. Chem., Int. Ed.* **2015**, *54*, 9001–9005.
(10) Liu, Y.; Moon, S.-Y.; Hupp, J. T.; Farha, O. K. *ACS Nano* **2015**, *9*, 12358–12364.
(11) Nguyen, H. G. T.; Mao, L.; Peters, A. W.; Audu, C. O.; Brown, Z. J.; Farha, O. K.; Hupp, J. T.; Nguyen, S. T. *Catal. Sci. Technol.* **2015**, *5*, 4444–4451.
(12) Li, Z.; Schweitzer, N. M.; League, A. B.; Bernales, V.; Peters, A. W.; Getsoian, A. B.; Wang, T. C.; Miller, J. T.; Vjunov, A.; Fulton, J. L.; Lercher, J. A.; Cramer, C. J.; Gagliardi, L.; Hupp, J. T.; Farha, O. K. *J. Am. Chem. Soc.* **2016**, *138*, 1977–1982.
(13) Peters, A. W.; Li, Z.; Farha, O. K.; Hupp, J. T. *ACS Nano* **2015**, *9*, 8484–8490.
(14) Yang, D.; Odoh, S. O.; Wang, T. C.; Farha, O. K.; Hupp, J. T.; Cramer, C. J.; Gagliardi, L.; Gates, B. C. *J. Am. Chem. Soc.* **2015**, *137*, 7391–7396.
(15) Nguyen, H. G. T.; Schweitzer, N. M.; Chang, C.-Y.; Drake, T. L.; So, M. C.; Stair, P. C.; Farha, O. K.; Hupp, J. T.; Nguyen, S. T. *ACS Catal.* **2014**, *4*, 2496–2500.
(16) Miner, E. M.; Fukushima, T.; Sheberla, D.; Sun, L.; Surendranath, Y.; Dinca, M. *Nat. Commun.* **2016**, *7*, 10942.
(17) Metzger, E. D.; Brozek, C. K.; Comito, R. J.; Dincă, M. *ACS Cent. Sci.* **2016**, *2*, 148–153.
(18) Comito, R. J.; Fritzsching, K. J.; Sundell, B. J.; Schmidt-Rohr, K.; Dinca, M. *J. Am. Chem. Soc.* **2016**, *138*, 10232–10237.
(19) Liu, T.-F.; Vermeulen, N. A.; Howarth, A. J.; Li, P.; Sarjeant, A. A.; Hupp, J. T.; Farha, O. K. *Eur. J. Inorg. Chem.* **2016**, *2016*, 4349–4352.
(20) Gutov, O. V.; Hevia, M. G.; Escudero-Adán, E. C.; Shafir, A. *Inorg. Chem.* **2015**, *54*, 8396–8400.
(21) Karunadasa, H. I.; Montalvo, E.; Sun, Y.; Majda, M.; Long, J. R.; Chang, C. J. *Science* **2012**, *335*, 698–702.
(22) Karunadasa, H. I.; Chang, C. J.; Long, J. R. *Nature* **2010**, *464*, 1329–1333.
(23) Luan, Y.; Qi, Y.; Yu, J.; Gao, H.; Schaus, S. E. *RSC Adv.* **2014**, *4*, 34199–34203.
(24) Mondloch, J. E.; Bury, W.; Fairen-Jimenez, D.; Kwon, S.; DeMarco, E. J.; Weston, M. H.; Sarjeant, A. A.; Nguyen, S. T.; Stair, P. C.; Snurr, R. Q.; Farha, O. K.; Hupp, J. T. *J. Am. Chem. Soc.* **2013**, *135*, 10294–10297.
(25) Rebsdat, S.; Mayer, D., Ethylene Oxide. In *Ullmann's Encyclopedia of Industrial Chemistry*, 7th ed.; VCH: Weinheim, Germany, 2012; Vol. *13*, pp 547–572.
(26) Thornburg, N. E.; Thompson, A. B.; Notestein, J. M. *ACS Catal.* **2015**, *5*, 5077–5088.
(27) Kwon, S.; Schweitzer, N. M.; Park, S.; Stair, P. C.; Snurr, R. Q. *J. Catal.* **2015**, *326*, 107–115.
(28) Han, X.-B.; Zhang, Z.-M.; Zhang, T.; Li, Y.-G.; Lin, W.; You, W.; Su, Z.-M.; Wang, E.-B. *J. Am. Chem. Soc.* **2014**, *136*, 5359–5366.
(29) Breysse, M.; Afanasiev, P.; Geantet, C.; Vrinat, M. *Catal. Today* **2003**, *86*, 5–16.

DOI: 10.1021/jacs.6b08898
J. Am. Chem. Soc. 2016, 138, 14720–14726

(30) Hermes, S.; Schröter, M.-K.; Schmid, R.; Khodeir, L.; Muhler, M.; Tissler, A.; Fischer, R. W.; Fischer, R. A. *Angew. Chem., Int. Ed.* **2005**, *44*, 6237−6241.
(31) Gu, X.; Lu, Z.-H.; Jiang, H.-L.; Akita, T.; Xu, Q. *J. Am. Chem. Soc.* **2011**, *133*, 11822−11825.
(32) Yuan, S.; Zou, L.; Li, H.; Chen, Y. P.; Qin, J.; Zhang, Q.; Lu, W.; Hall, M. B.; Zhou, H. C. *Angew. Chem., Int. Ed.* **2016**, *55*, 10776−10780.
(33) Neves, P.; Gomes, A. C.; Amarante, T. R.; Paz, F. A. A.; Pillinger, M.; Gonçalves, I. S.; Valente, A. A. *Microporous Mesoporous Mater.* **2015**, *202*, 106−114.
(34) Shylesh, S.; Jia, M.; Thiel, W. R. *Eur. J. Inorg. Chem.* **2010**, *2010*, 4395−4410.
(35) Sheldon, R. A.; Van Doorn, J. A. *J. Catal.* **1973**, *31*, 427−437.
(36) Joergensen, K. A. *Chem. Rev.* **1989**, *89*, 431−458.
(37) Sheldon, R. A.; Wallau, M.; Arends, I. W. C. E.; Schuchardt, U. *Acc. Chem. Res.* **1998**, *31*, 485−493.
(38) Shen, K.; Liu, X.; Lu, G.; Miao, Y.; Guo, Y.; Wang, Y.; Guo, Y. *J. Mol. Catal. A: Chem.* **2013**, *373*, 78−84.
(39) Nunes, C. D.; Valente, A. A.; Pillinger, M.; Rocha, J.; Gonçalves, I. S. *Chem. - Eur. J.* **2003**, *9*, 4380−4390.
(40) Nunes, C. D.; Valente, A. A.; Pillinger, M.; Fernandes, A. C.; Romao, C. C.; Rocha, J.; Goncalves, I. S. *J. Mater. Chem.* **2002**, *12*, 1735−1742.
(41) Jia, M.; Seifert, A.; Thiel, W. R. *Chem. Mater.* **2003**, *15*, 2174−2180.
(42) Imamura, S.; Sasaki, H.; Shono, M.; Kanai, H. *J. Catal.* **1998**, *177*, 72−81.
(43) Sakthivel, A.; Zhao, J.; Hanzlik, M.; Kuhn, F. E. *Dalton Trans.* **2004**, 3338−3341.
(44) Planas, N.; Mondloch, J. E.; Tussupbayev, S.; Borycz, J.; Gagliardi, L.; Hupp, J. T.; Farha, O. K.; Cramer, C. J. *J. Phys. Chem. Lett.* **2014**, *5*, 3716−3723.
(45) Stylianou, K. C.; Heck, R.; Chong, S. Y.; Bacsa, J.; Jones, J. T. A.; Khimyak, Y. Z.; Bradshaw, D.; Rosseinsky, M. J. *J. Am. Chem. Soc.* **2010**, *132*, 4119−4130.
(46) Klet, R. C.; Liu, Y.; Wang, T. C.; Hupp, J. T.; Farha, O. K. *J. Mater. Chem. A* **2016**, *4*, 1479−1485.
(47) Howarth, A. J.; Liu, Y.; Li, P.; Li, Z.; Wang, T. C.; Hupp, J. T.; Farha, O. K. *Nat. Rev. Mater.* **2016**, *1*, 15018.
(48) Mondloch, J. E.; Katz, M. J.; Isley Iii, W. C.; Ghosh, P.; Liao, P.; Bury, W.; Wagner, G. W.; Hall, M. G.; DeCoste, J. B.; Peterson, G. W.; Snurr, R. Q.; Cramer, C. J.; Hupp, J. T.; Farha, O. K. *Nat. Mater.* **2015**, *14*, 512−516.
(49) Wang, T. C.; Vermeulen, N. A.; Kim, I. S.; Martinson, A. B. F.; Stoddart, J. F.; Hupp, J. T.; Farha, O. K. *Nat. Protoc.* **2016**, *11*, 149−162.
(50) Hu, H.; Wachs, I. E.; Bare, S. R. *J. Phys. Chem.* **1995**, *99*, 10897−10910.
(51) Vuurman, M. A.; Wachs, I. E. *J. Phys. Chem.* **1992**, *96*, 5008−5016.
(52) Chae, B.; Jung, Y. M.; Wu, X.; Kim, S. B. *J. Raman Spectrosc.* **2003**, *34*, 451−458.
(53) Okamoto, Y.; Oshima, N.; Kobayashi, Y.; Terasaki, O.; Kodaira, T.; Kubota, T. *Phys. Chem. Chem. Phys.* **2002**, *4*, 2852−2862.
(54) Lezcano-González, I.; Oord, R.; Rovezzi, M.; Glatzel, P.; Botchway, S. W.; Weckhuysen, B. M.; Beale, A. M. *Angew. Chem., Int. Ed.* **2016**, *55*, 5215−5219.
(55) Leus, K.; Vandichel, M.; Liu, Y.-Y.; Muylaert, I.; Musschoot, J.; Pyl, S.; Vrielinck, H.; Callens, F.; Marin, G. B.; Detavernier, C.; Wiper, P. V.; Khimyak, Y. Z.; Waroquier, M.; Van Speybroeck, V.; Van Der Voort, P. *J. Catal.* **2012**, *285*, 196−207.
(56) Further reaction of an additional tBuOOH molecule does not significantly stabilize the node. See Figure S19.
(57) Hudson, M. J.; Knowles, J. A. *J. Mater. Chem.* **1996**, *6*, 89−95.
(58) Zhao, Y.; Truhlar, D. G. *J. Chem. Phys.* **2006**, *125*, 194101.
(59) Frisch, M. J.; Trucks, G. W.; Schlegel, H. B.; Scuseria, G. E.; Robb, M. A.; Cheeseman, J. R.; Scalmani, G.; Barone, V.; Mennucci, B.; Petersson, G. A.; Nakatsuji, H.; Caricato, M.; Li, X.; Hratchian, H. P.; Izmaylov, A. F.; Bloino, J.; Zheng, G.; Sonnenberg, J. L.; Hada, M.; Ehara, M.; Toyota, K.; Fukuda, R.; Hasegawa, J.; Ishida, M.; Nakajima, T.; Honda, Y.; Kitao, O.; Nakai, H.; Vreven, T.; Montgomery, J. A., Jr.; Peralta, J. E.; Ogliaro, F.; Bearpark, M.; Heyd, J. J.; Brothers, E.; Kudin, K. N.; Staroverov, V. N.; Kobayashi, R.; Normand, J.; Raghavachari, K.; Rendell, A.; Burant, J. C.; Iyengar, S. S.; Tomasi, J.; Cossi, M.; Rega, N.; Millam, J. M.; Klene, M.; Knox, J. E.; Cross, J. B.; Bakken, V.; Adamo, C.; Jaramillo, J.; Gomperts, R.; Stratmann, R. E.; Yazyev, O.; Austin, A. J.; Cammi, R.; Pomelli, C.; Ochterski, J. W.; Martin, R. L.; Morokuma, K.; Zakrzewski, V. G.; Voth, G. A.; Salvador, P.; Dannenberg, J. J.; Dapprich, S.; Daniels, A. D.; Farkas, Ö.; Foresman, J. B.; Ortiz, J. V.; Cioslowski, J.; Fox, D. J. *Gaussian 09*, Revision D; Gaussian, Inc.: Wallingford, CT, 2010.
(60) Zhao, Y.; Truhlar, D. G. *Acc. Chem. Res.* **2008**, *41*, 157−167.
(61) Zhao, Y.; Truhlar, D. G. *Chem. Phys. Lett.* **2011**, *502*, 1−13.
(62) Zhao, Y.; Truhlar, D. G. *J. Phys. Chem. C* **2008**, *112*, 6860−6868.
(63) Hehre, W. J.; Ditchfield, R.; Pople, J. A. *J. Chem. Phys.* **1972**, *56*, 2257−2261.
(64) Francl, M. M.; Pietro, W. J.; Hehre, W. J.; Binkley, J. S.; Gordon, M. S.; DeFrees, D. J.; Pople, J. A. *J. Chem. Phys.* **1982**, *77*, 3654−3665.
(65) Andrae, D.; Häußermann, U.; Dolg, M.; Stoll, H.; Preuß, H. *Theor. Chim. Acta* **1990**, *77*, 123−141.
(66) Marenich, A. V.; Cramer, C. J.; Truhlar, D. G. *J. Phys. Chem. B* **2009**, *113*, 6378−6396.

DOI: 10.1021/jacs.6b08898
J. Am. Chem. Soc. 2016, 138, 14720−14726